

SWAT-NN: Simultaneous Weights and Architecture Training for Neural Networks in a Latent Space

Zitong Huang

Department of Electrical & Computer Engineering
University of Southern California

Mansoorreh Montazerin

Department of Electrical & Computer Engineering
University of Southern California

Ajitesh Srivastava

Department of Electrical & Computer Engineering
University of Southern California

Abstract—Designing neural networks typically relies on manual trial and error or a neural architecture search (NAS) followed by weight training. The former is time-consuming and labor-intensive, while the latter often discretizes architecture search and weight optimization. In this paper, we propose a fundamentally different approach that simultaneously optimizes both the architecture and the weights of a neural network. Our framework first trains a universal multi-scale autoencoder that embeds both architectural and parametric information into a continuous latent space, where functionally similar neural networks are mapped closer together. Given a dataset, we then randomly initialize a point in the embedding space and update it via gradient descent to obtain the optimal neural network, jointly optimizing its structure and weights. The optimization process incorporates sparsity and compactness penalties to promote efficient models. Experiments on synthetic regression tasks demonstrate that our method effectively discovers sparse and compact neural networks with strong performance.

Index Terms—Neural Network Optimization, Functional Embedding, Autoencoder, Sparse Networks, Neural Architecture Search, Latent Space Optimization

I. INTRODUCTION

Traditionally, designing high-performing neural networks relies on a labor intensive and trial-and-error approach, which generally consists of defining a fixed architecture, training the weights of the network, evaluating performance, and iteratively refining the architecture to achieve better results. This iterative cycle is time-consuming, computationally expensive, and highly dependent on expert intuition.

To address this challenge, Neural Architecture Search (NAS) has emerged as a promising framework for automatically discovering effective neural network architectures [1], [2]. Existing NAS methods can be broadly classified into discrete and continuous search approaches. Early NAS methods predominantly employed Reinforcement Learning (RL) [3] and evolutionary algorithms [4], [5], which fall under the discrete search category. RL-based methods [6], [7] formulate architecture design as a sequential decision-making process, where

each component of the architecture is treated as an action, and the objective is to find a sequence of actions that maximizes performance. Alternatively, evolutionary algorithms [8]–[10] search by iteratively mutating and recombining candidate operations to evolve better-performing architectures. Despite their differences, both approaches operate over high-dimensional discrete representations and navigate a vast combinatorial search space defined by a predefined set of operations. In contrast to discrete strategies, continuous NAS methods [2], [11] have gained attention for their efficiency and ability to operate in a differentiable search space [12]–[14]. These methods create a continuous (e.g., softmax) version of the decision objective, enabling search via gradient descent. The architecture is typically modeled as a computational graph, where each edge carries a soft weight over a predefined set of candidate operations. Nevertheless, while continuous NAS methods significantly reduce search cost and enable differentiable optimization, they are often constrained by task-specific predictors or datasets, and typically search for architectures and weights in a decoupled or alternating manner.

In this work, we propose SWAT-NN, which jointly optimizes both the architecture and its corresponding weights to achieve high performance on given datasets. It is based on a multi-scale autoencoder framework, trained to embed functionally similar neural networks close to one another within a continuous latent space. The encoder learns to represent the full neural network – including both its structure and parameters – in an embedding space, from which multiple decoders generate functionally similar neural networks of varying depths. This embedding, once trained, enables gradient-based optimization (with respect to the embedding, instead of weights) by directly optimizing task-specific performance. Because the latent representation jointly encodes architecture and weights, our method performs unified optimization over both, without requiring separate architectural parameters or surrogate models. We evaluate our proposed approach in the

context of multi-layer perceptrons (MLPs) with three different activation functions: sigmoid, tanh, and leaky ReLU, and apply it to the Continuous Optimization Benchmark Suite from Neural Network Regression (CORNN) dataset, which contains 54 regression tasks derived from diverse benchmark functions [15]. Notably, the proposed approach diverges from conventional NAS paradigms by treating networks holistically as function approximators, rather than representing them as graphs composed of discrete operations. This allows the embedding to be over their actual functional behavior. Our main contributions can be summarized as follows:

- 1) We propose a new framework, SWAT-NN, that performs simultaneous optimization over neural network architectures and weights within a universal embedding space, departing fundamentally from traditional NAS methods that decouple architecture search and weight tuning.
- 2) We show that SWAT-NN supports fine-grained architecture discovery, including neuron-level activation function selection and layer-wise width adaptation.
- 3) Through extensive experiments on 54 regression tasks, we show that SWAT-NN discovers significantly sparser and more compact models compared to existing methods, while maintaining comparable or better accuracy.

II. RELATED WORK

Neural networks can be designed manually or through automated search techniques known as Neural Architecture Search (NAS). Traditional NAS approaches include reinforcement learning (RL) [3] or evolutionary algorithms [4], [5]: RL formulates architecture design as a sequential decision-making process, whereas evolutionary methods construct architectures by iteratively mutating or recombining predefined operations. However, these methods typically operate in a discrete search space, making them computationally expensive and difficult to scale. More recent efforts explore continuous NAS, which relaxes the discrete architecture space into a continuous domain.

Differentiable Architecture Search (DARTS) [11] is one of the most influential gradient-based NAS methods. It relaxes discrete architectural choices by introducing a softmax over all candidate operations on each edge of a directed acyclic graph (DAG). The search process is framed as a bi-level optimization problem, in which the network weights are optimized on the training set, while the architecture parameters are updated on the validation set. Such decoupling breaks joint optimization and can result in suboptimal architectures due to misaligned objectives between weight and architecture updates.

Neural Architecture Optimization (NAO) based on a graph variational autoencoder (VAE) [16] encodes network architectures into a continuous latent representation specific to the given set of datasets. It uses a surrogate performance predictor, a regression model estimating task-specific accuracy of an architecture based on its latent representation, to guide the search. Specifically, it performs gradient ascent in the latent space to find architectures that are predicted to perform well for the given dataset. While NAO improves the smoothness of

the optimization landscape and captures mathematical properties of architectures through its encoder, it fully decouples architecture discovery from weight optimization and relies on dataset-specific autoencoder and predictors.

In contrast, we propose a novel approach that departs fundamentally from conventional NAS formulations. Rather than searching over discrete or graph-based compositions of operations, we treat entire neural networks as function approximators and embed their complete mathematical behavior – including both architecture and weights – into a universal continuous latent space. Optimization is performed directly on this functional representation, without relying on manually defined search spaces or architectural priors. Moreover, our method is agnostic to specific datasets, as it does not depend on task-specific performance predictors or surrogate models, enabling more general and flexible network discovery. Unlike many the existing methods, which generate the networks through a sequence of decisions [4]–[7], [16], our approach decodes a complete neural network from a point in the embedding space.

III. METHODOLOGY

The key idea of SWAT-NN is based on achieving the following two goals (see Fig. 1): (1) training a multi-scale autoencoder to construct a latent embedding space for multi-layer perceptrons (MLPs) (Section III-A); and (2) searching for sparse and compact networks via gradient descent in the learned embedding space (Section III-B). This paper focuses on training MLPs with a varying number of neurons per layer and different activation functions per neuron.

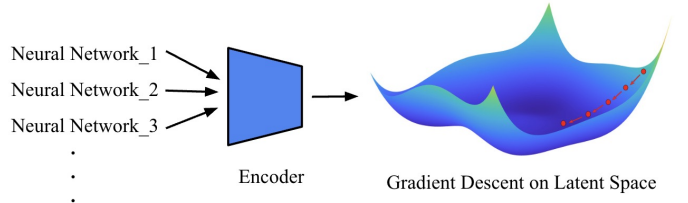


Fig. 1. An illustration of the overall idea for SWAT-NN

A. Embedding MLPs with Autoencoder

We aim to encode both the architecture and corresponding weights of a neural network into a shared embedding space [17]. This is achieved through a multi-scale autoencoder framework. The encoder, denoted as E , maps a given MLP into a latent representation. A set of L decoders, denoted as D_1, D_2, \dots, D_L , then, generate MLPs with 1 to L hidden layers, respectively. The autoencoder is trained to generate MLPs that may not be reconstructions of the input networks, but are functionally similar – that is, they produce similar outputs when given the same inputs. In the following, we provide further details on the MLP representation and autoencoder design:

1) *Matrix Representation of MLPs*: To train an autoencoder for encoding neural networks, we require a structured and fixed-size representation of MLPs that can act as input. Both the architecture and weights of an MLP are encoded in a concise matrix-based representation. For an MLP with L hidden layers, each containing N neurons, input dimension i , and output dimension o , the weights between consecutive layers can be expressed as a sequence of matrices:

$$[(W_{i,N}, b_N), (W_{N,N}, b_N), \dots, (W_{N,N}, b_N), (W_{N,o}, b_o)] \quad (1)$$

where $W_{i,N} \in \mathbb{R}^{i \times N}$, $W_{N,N} \in \mathbb{R}^{N \times N}$, and $W_{N,o} \in \mathbb{R}^{N \times o}$ are weight matrices between layers, and the corresponding bias vectors are $b_N \in \mathbb{R}^{N \times 1}$, $b_o \in \mathbb{R}^{o \times 1}$. To ensure uniform dimensionality for concatenation, we apply zero-padding to the first and last matrices so that all matrices have dimensions of $N \times N$. In addition, each bias vector is padded to $N \times 1$ and horizontally concatenated into the matrix of weights. To differentiate between the actual weights and padded entries, a secondary mask matrix is appended in parallel to the matrix described above. More specifically, each position corresponding to an original MLP weight is assigned a value of 1 in the mask, while positions introduced through zero-padding are assigned a value of 0. The sizes of the input and output layers can also be flexibly specified using boundary-layer masks (see Section V-F). This basic representation is later extended to incorporate varying numbers of neurons and activation functions in Section III-A3 and Section III-A4; an overview of the complete representation scheme is illustrated in Fig. 3.

2) *Multi-scale Autoencoder*: The multi-scale autoencoder consists of a single encoder E and decoders D_1, D_2, \dots, D_L , where each decoder D_k generates an MLP with k hidden layers. The overall structure is illustrated in Fig. 2.

The encoder and decoders are implemented using a GPT-2 architecture [18]. Following the matrix representation of MLPs described in Section III-A1, each row h corresponds to the concatenation of all outgoing weights from the h^{th} neuron across every layer of the MLP. In other words, the h^{th} row aggregates the weights from the h^{th} neuron in each layer to all neurons in the subsequent layers, providing a unified view of its outgoing connections throughout the network. Accordingly, we treat the set of outgoing weights from the h^{th} neuron across all layers as a single unified token. Each row h is, then, linearly projected to be compatible with the token embedding size of the GPT-2 encoder and decoders. This representation bounds the number of tokens by the maximum number of neurons per layer, thereby minimizing computational cost. By concatenating outgoing weights across layers, the model is further enabled to capture long-range dependencies.

During the encoding stage, the MLP matrix representation is provided as input to the encoder, which maps it to a latent embedding. This embedding is then passed to L decoders, each corresponding to a different target MLP depth. In the decoding stage, each decoder uses a GPT-2-style autoregressive generation process to produce a new matrix representation of an MLP. For decoder D_k , we retain only the first k hidden-layer

blocks from the generated output matrix, yielding the final representation of an MLP with k hidden layers.

3) *Varying Number of Neurons*: To enable the autoencoder to account for different numbers of neurons per layer as part of the network architecture, we introduce a neuron indicator matrix to explicitly encode this structural variation. For an MLP with L hidden layers, each with at most N neurons, we augment the matrix representation introduced in Section III-A1 by appending an additional mask matrix $M \in \{0, 1\}^{N \times L}$. Each column of M corresponds to one hidden layer, which indicates the activation status of all the neurons in that layer. Specifically, $M_{h,j} = 1$ if the h^{th} neuron in the j^{th} hidden layer is active in the input MLP, and $M_{h,j} = 0$ otherwise.

We apply the autoencoder introduced in Section III-A2 to this extended representation. The decoded neuron indicator matrix $\hat{M} \in [0, 1]^{N \times L}$ is obtained via a sigmoid activation, where each element $\hat{M}_{h,j}$ represents the probability of the h^{th} neuron in the j^{th} hidden layer being active. To preserve the differentiability of the loss function during training, we avoid hard thresholding for enforcing binary activations. Instead, we use a soft thresholding method to decide entirely active vs pruned neurons described in Section III-B2.

4) *Changing Activation Functions*: To capture activation function choices as part of the network architecture, we extend the matrix representation to explicitly encode which activation function is applied to each neuron. We incorporate activation function choices into the matrix representation introduced in Section III-A1 and Section III-A3 through appending additional columns that specify the activation function used by each neuron. Assuming a total of A possible activation functions, the activation type of each neuron is encoded as a one-hot vector of length A . The final representation is:

$$[(W_{i,N}, b_N), F_{N,A}, (W_{N,N}, b_N), F_{N,A}, \dots, (W_{N,N}, b_N), F_{N,A}, (W_{N,o}, b_o), M_{N,L}] \quad (2)$$

The final matrix $M_{N,L} \in \{0, 1\}^{N \times L}$ indicates neuron activity as described in Section III-A3. Each $F_{N,A} \in \{0, 1\}^{N \times A}$ follows a hidden layer's weight and bias matrix and encodes the activation function for each neuron in that layer. An illustration of the whole matrix representation is shown in Fig. 3.

After feeding the extended representation into the encoder-decoder framework, we apply continuous relaxation to decoded $\hat{F}_{N,A}$ matrices to enable differentiable selection of activation functions. Each row of $\hat{F}_{N,A}$ is interpreted as a softmax distribution over the A candidate activation functions. Formally, for a neuron h in layer j , the output is computed as a soft combination of candidate activation functions:

$$y_{(h,j)}(x) = \sum_{k=1}^A \alpha_{(h,j),k} \cdot o_k(x) \quad (3)$$

where x is the input flows through current neuron (h, j) , and $o_k(\cdot) \in \mathcal{O}$ denotes the k^{th} candidate activation function from a

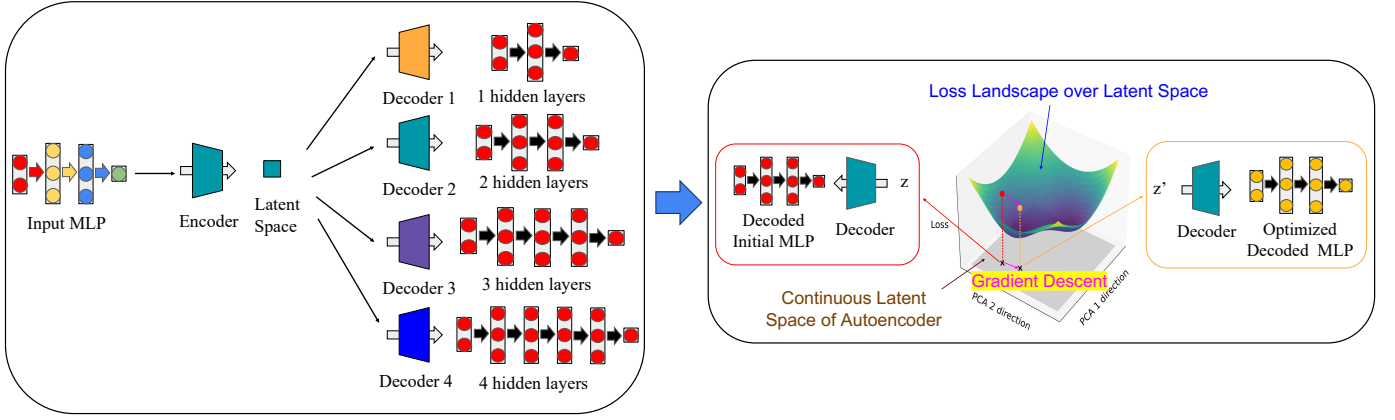


Fig. 2. Left: Multi-scale autoencoder architecture with four decoders, each corresponding to MLPs with 1–4 hidden layers. Right: Pipeline for training optimal MLPs through gradient-based optimization in the continuous latent space learned by the autoencoder.

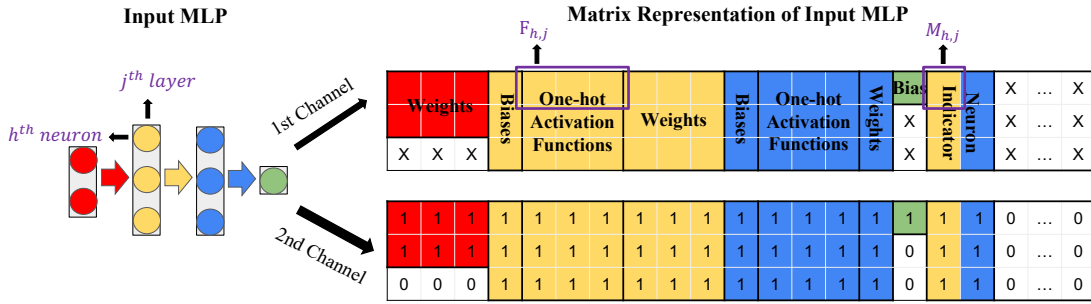


Fig. 3. Matrix representation for a 2 hidden-layer MLP with 3 neurons per layer. Different colors indicate elements associated with neurons from different layers, encoding the outgoing weights, activation functions, and bias terms of each neuron. Entries marked with 'X' represent zero-padding.

predefined activation function set \mathcal{O} . The activations' selection probabilities are given by:

$$\alpha_{(h,j),k} = \text{softmax}(\hat{F}_{h,:}^{(j)})_k \quad (4)$$

Here, $\hat{F}_{h,:}^{(j)} \in \mathbb{R}^A$ denotes the decoded activation logits for the h^{th} neuron in the j^{th} hidden layer. This relaxation preserves differentiability during training, enabling smooth optimization over activation selections. A near-discrete activation assignment can be enforced at inference time in Section III-B3.

5) *Training Autoencoder*: We generate input vectors x , and feed them into the input MLP \mathcal{N}_s to obtain the corresponding outputs. Each input MLP is then passed through the autoencoder to produce decoded MLPs with varying depths $\{1, 2, \dots, L\}$. We adopt a minimum-loss objective to encourage functional similarity between the input MLP and its decoded variants [17]. The loss function is defined as:

$$L_{ED} = \sum_{\mathcal{N}_s} \min_{i \in \{1, 2, \dots, L\}} \left(\sum_x (\mathcal{N}_s(x) - [D_i(E(\mathcal{N}_s))](x))^2 \right) \quad (5)$$

where $\mathcal{N}_s(x)$ denotes the output of the original input MLP evaluated at input x , and $[D_i(E(\mathcal{N}_s))](x)$ denotes the output of the decoded MLP with i hidden layers, reconstructed from the embedding and evaluated at the same input x . This objective encourages at least one decoded MLP to closely

approximate the functional behavior of the original MLP across all sampled inputs. It effectively pulls functionally similar MLPs closer together in the embedding space.

The runtime complexity for training a single encoder and L decoders is $\mathcal{O}(E \cdot \frac{N}{B} \cdot L \cdot f)$, where f is the cost of a forward and backward pass through GPT-2, N is the dataset size, B is the batch size, and E is the number of training epochs.

B. Training MLP in the Embedding Space

Given a dataset S , we leverage the multi-scale autoencoder, where functionally similar MLPs are smoothly embedded close to each other, to search for a sparse and compact MLP tailored to S . The decoded MLP can vary in the number of hidden layers (up to L), the number of neurons per layer (up to N), sparsity patterns, and activation functions across neurons (selected from \mathcal{O}). All architectures lie within the structural constraints defined during autoencoder training.

1) *Training Optimal MLPs for a Dataset*: The learnable parameters of the multi-scale autoencoder described above are fixed during this stage. Since all MLPs are embedded into a continuous latent space, the problem of finding an optimal MLP reduces to optimizing an embedding vector $z \in \mathbb{R}^d$ within this space. Given a dataset $S = \{(x, y)\}$, we define

the objective function for decoder D_i as:

$$L_i(z) = \sum_{(x,y) \in S} ([D_i(z)](x) - y)^2 \quad (6)$$

where $[D_i(z)](x)$ denotes the output of the decoded MLP with i hidden layers evaluated at input data x . The gradient of L_i with respect to z can be written as:

$$\nabla_z L_i = 2 \sum_{(x,y) \in S} ([D_i(z)](x) - y) \nabla_z [D_i(z)](x) \quad (7)$$

To solve this optimization problem, we initialize z by randomly sampling an embedding vector, and performing gradient descent to minimize $L_i(z)$ with respect to z . Specifically, the update rule can be defined as:

$$z^{(t+1)} = z^{(t)} - \eta \frac{\partial L_i}{\partial z^{(t)}} \quad (8)$$

where η is the learning rate and $t \in \{0, 1, \dots, T\}$ denotes the optimization step. The runtime complexity for this optimizing is $\mathcal{O}(L \cdot T \cdot f)$, where L is the number of decoders, T is the number of gradient steps per decoder, and f is the cost of a forward and backward pass through a GPT-2 decoder.

2) *Sparsity and Compactness*: To promote neural networks that are both sparse (fewer connections) and compact (fewer active neurons), we incorporate two regularization terms into the loss: a weight sparsity penalty \mathcal{P}_s to drive individual weights toward zero, and a neuron compactness penalty \mathcal{P}_n to suppress redundant neurons and promote compact architectures. The overall loss function is defined as:

$$L_i(z) = \sum_{(x,y) \in S} ([D_i(z)](x) - y)^2 + \lambda_s \cdot \mathcal{P}_s + \mathcal{P}_n \quad (9)$$

where \mathcal{P}_s denotes the sparsity penalty weighted by coefficients λ_s , and \mathcal{P}_n denotes the neuron compactness penalty.

Sparsity Penalty. \mathcal{P}_s consists of two components: an ℓ_1 -regularization term and a soft counting switch. Formally, it is defined as:

$$\mathcal{P}_s = \mathcal{L}_1 + \text{SoftCount}, \quad (10)$$

$$\text{Where, } \mathcal{L}_1 = \mu_1 \|W[D_i(z)]\|_1, \quad (11)$$

$$\text{And, } \text{SoftCount} = \mu_c \cdot \sigma(20 \cdot \|W[D_i(z)]\|_1 - t_s) \quad (12)$$

Here, $W[D_i(z)]$ denotes the weight matrix of the decoded MLP $D_i(z)$, and t_s is a learnable threshold parameter. The \mathcal{L}_1 term encourages weights to shrink toward zero. The soft counting switch approximates the number of weights below the threshold t_s , using a scaled sigmoid function to softly suppress small-magnitude weights. During training, weights smaller than t_s are softly masked using a sigmoid-based function that smoothly pushes them toward zero; at test time, they are hard-masked. Both μ_1 and μ_c are tunable hyperparameters that control the relative strength of ℓ_1 regularization and the soft counting penalty, respectively.

Neuron Compactness Penalty. To reduce the number of active neurons per layer by pruning unnecessary ones, we define the neuron compactness penalty \mathcal{P}_n as a combination

of two terms: the negative variance and the average magnitude of soft activation masks across neurons within each layer:

$$\mathcal{P}_n = -\alpha \cdot \frac{1}{L} \sum_{i=1}^L \text{std}(M_i) + \beta \cdot \frac{1}{L} \sum_{i=1}^L \text{mean}(M_i) \quad (13)$$

Here, M_i denotes the soft neuron activation indicators for the i^{th} hidden layer, and L is the number of hidden layers. The first term encourages the activation probabilities within each layer to become more polarized, while the second term penalizes the average activation level to further suppress unnecessary neurons. Coefficients α and β are hyperparameters controlling the strength of each term. During training, neuron indicators smaller than a fixed threshold $t_n = 0.5$ are softly masked using a sharpened sigmoid function that closely approximates hard thresholding while maintaining differentiability; at test time, neurons this threshold are hard-masked as inactive.

3) *Activation Function Selection*: We adopt a temperature-controlled softmax mechanism [11] to gradually fix the activation function assigned to each neuron. We define a temperature schedule over training epochs as follows:

$$T(e) = \max \left(T_{\text{final}}, T_{\text{init}} \cdot \left(1 - \frac{e}{E_{\text{anneal}}} \right) \right) \quad (14)$$

Here, T_{init} is the temperature at the beginning of training, T_{final} is the minimum temperature reached. E_{anneal} is the number of epochs over which the temperature linearly decays to T_{final} , and e denotes the current training epoch.

During training, for each neuron, a softmax over activation function candidates (i.e., Leaky ReLU, Tanh, Sigmoid) is applied using the current temperature $T(e)$. Let $\mathbf{a}_{h,j} \in \mathbb{R}^A$ denote the unnormalized logits for A activation candidates of the h^{th} neuron in layer j ; the contribution weight of activation operation a at neuron (h, j) is computed as:

$$\alpha_{(h,j),k} = \frac{\exp(\mathbf{a}_{(h,j),k}/T(e))}{\sum_{k=1}^A \exp(\mathbf{a}_{(h,j),k}/T(e))} \quad (15)$$

As training progresses and $T(e)$ decreases, the softmax distribution sharpens, eventually approximating a one-hot selection. At test time, we select the activation function with the highest softmax score for each neuron as its final activation.

IV. EXPERIMENTS AND RESULTS

Our experiments are structured into three components:

- **Exp 1: Learning Sparse and Compact MLPs (Joint Optimization of Activation, Neuron Usage, and Sparsity).** We evaluate SWAT-NN, which simultaneously optimizes activation functions, neuron usage, and weight sparsity. We compare against DARTS, a baseline that supports differentiable architecture search, followed by Alternating Direction Method of Multipliers (ADMM) pruning [19].
- **Exp 2: Search for Activation Functions.** To isolate the effect of neuron-level activation function selection, we evaluate our framework described in Section III-B3 and

compare it against two baselines: (a) autoencoder-based search with fixed activation functions, and (b) traditional MLP training with fixed activation functions.

- **Exp 3: Search for Sparse MLPs.** To further isolate the effect of weight sparsity, we fix neuron counts and optimize for sparse weights, as described in Section III-B2. We compare against a baseline where autoencoder-based search is followed by ADMM pruning.

All the code is publicly available ¹.

1) *Dataset:* All evaluations are conducted on the CORNN dataset [15], which consists of 54 synthetic regression tasks. Each task defines a distinct function $f : \mathbb{R}^2 \rightarrow \mathbb{R}$, designed to capture a wide range of functional behaviors, including periodicity, discontinuities, sharp curvature, and varying smoothness. For each task, the data is split into 3,750 training samples and 1,250 test samples. All inputs are normalized to lie within $[-1, 1]^2$, and outputs are scaled to the range $(-1, 1)$.

2) *Autoencoder Settings:* We trained a multi-scale GPT-2 autoencoder with one encoder and four decoders for MLPs with 1-4 hidden layers. Each input MLP has two inputs, one output, and up to 7 neurons per hidden layer. Weights and biases are sampled from $[-5, 5]$ and $[-1, 1]$, respectively. For each MLP, 1000 inputs are uniformly sampled from $[-1, 1]^2$, and the autoencoder is trained using the loss function in Section III-A5. Each training epoch includes 50,000 batches (batch size 64) and takes around 3 hours to complete on a single RTX A5000 GPU. In Section V-F, we also incorporate varying input and output dimensions by applying the same masking and padding strategy to the boundary layers.

3) *Baselines:* Most NAS methods do not perform truly simultaneous optimization of both architecture and weights. Instead, they decouple the process and are dataset-specific. In contrast, our method jointly optimizes structure and parameters in a universal embedding space, enabling direct gradient-based optimization for sparse and performant neural networks.

Exp 1: DARTS with ADMM Although no prior work jointly optimizes both architecture and weights, we compare against a baseline, evaluated in Section IV-A, that adapts DARTS to MLPs, allowing differentiable search over number of neurons per layer and neuron-level activation functions. The resulting architecture is then pruned using ADMM, an optimization method that alternates between minimizing loss and enforcing sparsity via auxiliary variables and dual updates.

The DARTS search space is a directed acyclic graph (DAG), where each node represents a layer-wise feature, and each edge encodes a candidate layer configuration defined by neuron count and activation functions. Softmax relaxation enables gradient-based optimization of both. Unlike the original DARTS designed for CNNs or RNNs, we omit cell repetition and reduction layers, as these are not applicable to fully connected MLPs without spatial or sequential hierarchies.

We train the DARTS model for 50 epochs to search for the architecture using bilevel optimization [11] procedure. ADMM is then applied with $\rho = 2$ and a threshold of 10^{-1} to

sparsify the weights. These hyperparameters are selected after increasing sparsity strength until performance on roughly one-third of the tasks dropped over 5% – our tolerable limit.

Exp 2: Autoencoder-based Search with Fixed Activation Functions Used as a baseline in Section IV-B, we fix the activation function for all neurons to one of Sigmoid, Tanh, or Leaky ReLU, and use the trained autoencoder to optimize over weights (8000 epochs, learning rate 0.1).

Exp 2: Traditional MLP Training Also evaluated in Section IV-B, we train MLPs with fixed activation functions and randomly initialized weights using standard gradient descent for 6000 epochs at a learning rate of 0.01. This reflects a common trial-and-error approach.

Exp 3: Autoencoder with ADMM Used as a baseline in Section IV-C, we combine autoencoder-based architecture and weight optimization without sparsity penalty with post-hoc ADMM pruning. Models are trained for 8000 epochs with a learning rate of 0.1, while the ADMM uses $\rho = 2$ and a pruning threshold of 10^{-1} .

A. Learning Sparse and Compact MLPs (Joint Optimization of Activation, Neuron Usage, and Sparsity)

In SWAT-NN setting, for sparsity penalty, we set λ_s to 1×10^{-4} , $\mu_1 = 0.1$ for the ℓ_1 penalty and $\mu_c = 0.01$ for the soft count term. For neuron compactness penalty, we use $\alpha = 0.4$ and $\beta = 0.001$. For activation function selection, we set $T_{\text{init}} = 1.0$, $T_{\text{final}} = 0.01$, $E_{\text{anneal}} = 3000$. These hyperparameters are tuned using the last two benchmark functions (F53 and F54) from the CORNN dataset as a validation set. SWAT-NN training takes about 1 minute per task and per MLP configuration on a machine with a single RTX A5000 GPU, 128GB RAM, and a 56-core CPU.

Fig. 4 presents MSE vs non-zero weights for 28 benchmark functions, where each point represents a model configuration, and positions closer to the bottom-left indicate lower MSE and higher sparsity. SWAT-NN always identifies solutions closer to the optimal accuracy-sparsity trade-off, demonstrating its advantage in producing more compact and efficient networks.

Fig. 5 show the results on all dataset in terms of MSE and number of non-zero weights. For each function, we apply a two-step selection criterion: we first identify architectures whose MSE is within 5% of the minimum, and among them select the one with the fewest non-zero weights. While SWAT-NN and DARTS followed by ADMM achieve similar test accuracy, in most cases, SWAT-NN consistently discovers models with significantly fewer non-zero weights.

B. Search for Optimal MLPs with Activation Functions

We focus exclusively on the search over activation functions. We use all 7 neurons in each hidden layer and do not apply the sparsity penalty discussed in Section III-B2 during training. The same hyperparameters for activation function selection are used as described in the Section IV-A experiment. Each experiment is repeated three times, and we report the average MSE across runs.

¹<https://tinyurl.com/SWAT-NN>

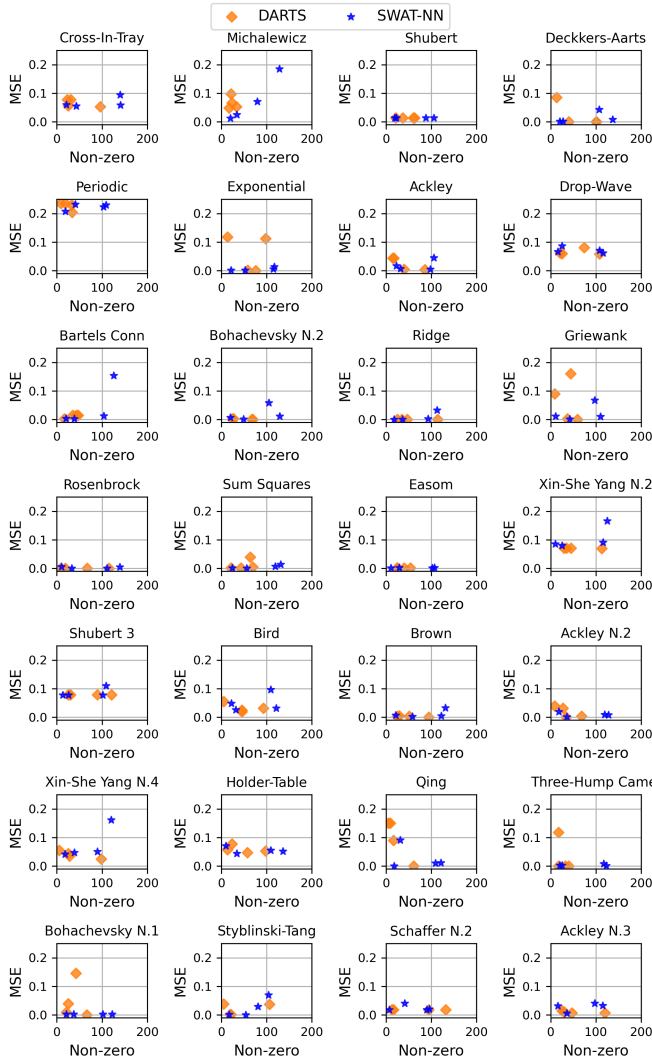


Fig. 4. MSE vs non-zero weights between DARTS+ADMM and SWAT-NN across 28 randomly selected benchmark functions. Each point represents a model configuration, plotted by its test MSE and number of non-zero weights.

We compare our method, which searches neuron-level activation functions in the embedding space, with autoencoder-based search with fixed activation functions described in Section IV-3. As shown in Fig. 6, our method consistently achieves performance comparable to or better than the best fixed-activation baselines, demonstrating that searching over activation types improves model performance.

Fig. 7 further compares our method to the traditional training baseline described in Section IV-3. Our method achieves performance comparable to MLPs trained using traditional training method with fixed activation functions in most cases. While the accuracy is similar, the ability to flexibly assign activation functions per neuron enables our method to produce more compact and sparse networks, as demonstrated in Section IV-A and Section IV-C.

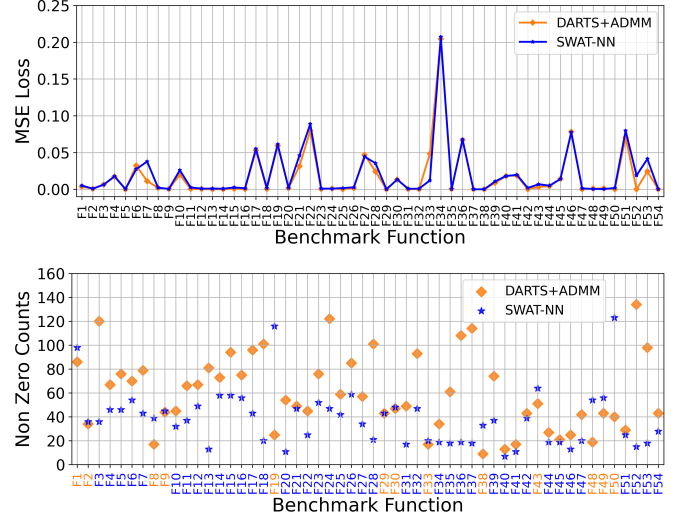


Fig. 5. Top: Test MSE of the best-performing models identified by DARTS+ADMM and SWAT-NN across all 54 functions. Bottom: Corresponding number of non-zero weights. Function labels are color-coded to indicate which method yields a more sparse and compact model.

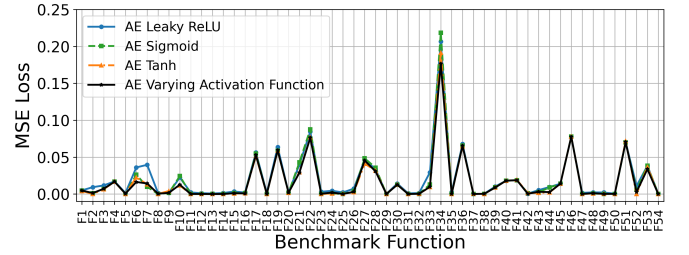


Fig. 6. Comparison of MSE using autoencoder-based search with fixed activation functions versus neuron-level activation function search.

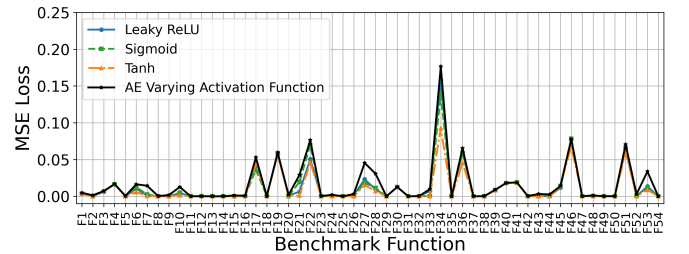


Fig. 7. Comparison of the best MSEs obtained by traditional training baseline using Leaky ReLU, Sigmoid, and Tanh activations versus autoencoder-searched MLPs with neuron-level activation functions.

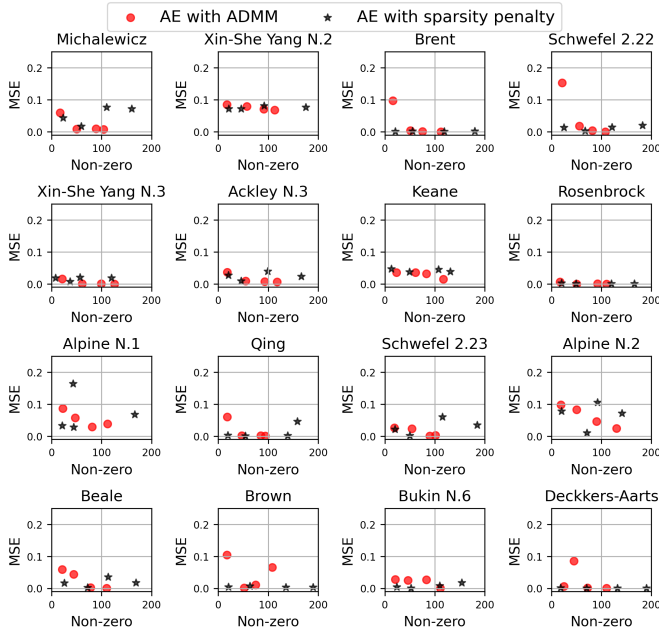


Fig. 8. MSE vs. non-zero weights for autoencoder-based search with ADMM and with sparsity penalties. Each point represents a model configuration.

C. Search for Sparse MLPs

Building upon the activation function search in Section IV-B, we compare our autoencoder-based search incorporated with sparsity penalties with the baseline of autoencoder-based search with ADMM afterwards described in Section IV-3. For our autoencoder-based method, we set λ_s to 1×10^{-3} , and use $\mu_1 = 0.1$ for the ℓ_1 penalty and $\mu_c = 0.01$ for the soft count term. Note that in this set of experiments, we do not apply neuron-level pruning yet.

The MSE vs non-zero weights scatter plots for 16 benchmark functions shown in Fig. 8 indicates that our method consistently produces configurations that dominate or closely approach the left-down corner region. Meanwhile, Fig. 9 summarize the best selected model configurations in terms of MSE and number of non-zero weights. Compared to the models without any pruning, our autoencoder-based method with sparsity penalties achieves substantial reductions in non-zero weights while maintaining similar MSE. Furthermore, relative to the baseline where autoencoder-based search is followed by ADMM pruning, our simultaneous search consistently identifies more compact models. In most cases, it also achieves lower or comparable test MSE, demonstrating the effectiveness of integrating sparsity directly into the optimization process rather than decomposing architecture discovery and weight training or pruning into separate stages.

V. DISCUSSION

A. Smoothness of the Embedding Space

The embedding space learned by the multi-scale autoencoder is central to our framework, mapping functionally similar MLPs to nearby points in the embedding space.

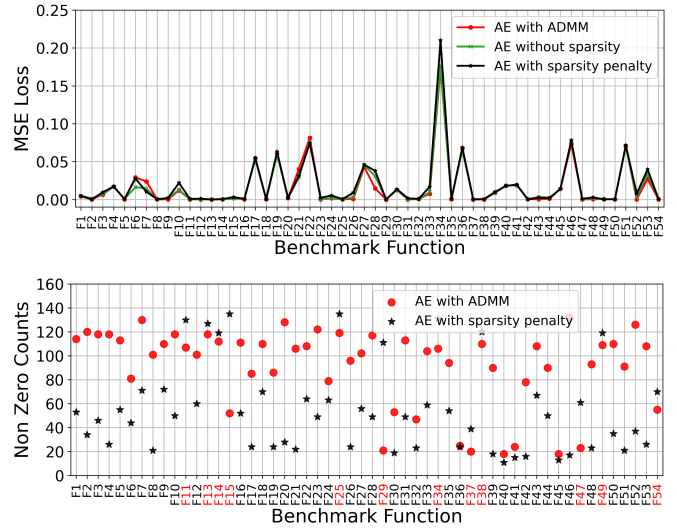


Fig. 9. Top: MSE of the best-performing models, comparing AE followed by ADMM, AE followed by sparsity penalty, and AE without pruning. Bottom: Corresponding number of non-zero weights in the selected models. Function labels are color-coded to indicate which method yields a sparse model.

A smooth embedding space enables accurate gradient-based navigation toward optimal networks. To assess smoothness of the embedding space for each decoder D_k , we sample a base embedding vector $z_{\text{init}} \sim \mathcal{N}(0, I)$ and generate 200 nearby embeddings by adding small Gaussian noise. We then apply principal component analysis (PCA) and extract the top two principal directions, denoted v_1 and v_2 . These directions define a local 2D subspace around z_{init} , along which we generate perturbed embeddings $z' = z_{\text{init}} + \alpha v_1 + \beta v_2$, where $\alpha, \beta \in [-3, 3]$ are sampled on a grid.

Each perturbed embedding z' , along with z_{init} , is decoded using D_k to obtain the corresponding decoded MLPs. For a fixed set of input values, we compute the outputs of $D_k(z_{\text{init}})$ and $D_k(z')$, treating the former as ground truth. The MSE between the two outputs quantifies the functional deviation induced by perturbations in the embedding space.

We visualize the resulting MSE values over the 2D grid of (α, β) to assess the smoothness of the embedding space. Fig. 10 shows that the MSE varies smoothly across directions v_1 and v_2 , indicating that the latent space learned by the autoencoder preserves functional continuity.

B. Comparison Between CNN-Based and GPT-Based Autoencoders

A prior work [17] used a CNN-based autoencoder. In this work, we use a GPT-based autoencoder, which we find more effective at capturing functional representations. Both autoencoders are trained under the same basic setting – without bias terms, neuron masking, or activation function selection (all neurons use sigmoid). Using the same training configuration, we compare the best MSE achieved in downstream MLP search on CORNN dataset. As shown in Fig. 11, the GPT-based model consistently outperforms the CNN-based one.

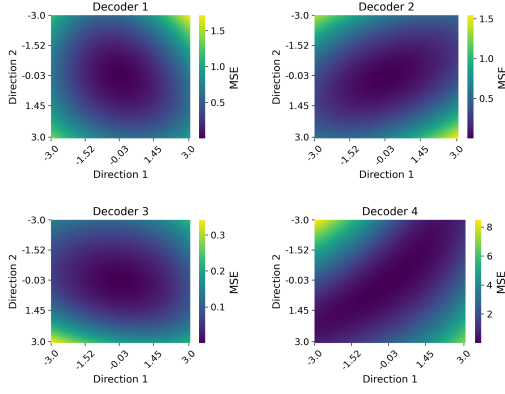


Fig. 10. Visualization of latent space smoothness across 2D subspaces for the four decoders.

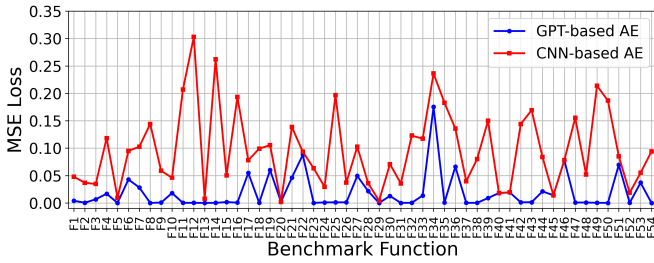


Fig. 11. Comparison of minimum test MSE across benchmark functions using CNN-based and GPT-based autoencoders.

C. Functional Approximation by the Autoencoder

We visualize the decoded outputs corresponding to input MLPs with 1 to 4 hidden layers, as shown in Fig. 12. While the decoded MLPs generally approximate the functional behavior of the inputs, some discrepancies remain, particularly for deeper networks. However, as demonstrated in Section IV, our method is still able to discover high-performing MLPs through gradient-based optimization in the embedding space.

We hypothesize that this is because the embedding space only needs to provide a sufficiently smooth and semantically organized landscape, such that gradient descent can navigate toward better-performing regions. The autoencoder does not need to achieve perfect reconstruction, but rather serve as a functional embedding mechanism. Improving the fidelity of the autoencoder would further enhance the smoothness and precision of the search space, leading to improved performance in the downstream optimization.

D. Different hyperparameter choices

In Equation 9, Equation 10, and Equation 13, the sparsity and compactness behavior of the searched neural networks is primarily governed by three key hyperparameters: λ_s for controlling the overall strength of sparsity, and the internal weighting coefficients α and β used in the neuron compactness term. We evaluate three settings with increasing regularization strength, as summarized in Table I.

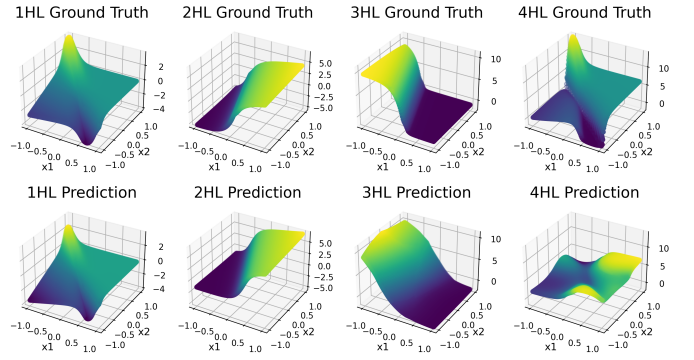


Fig. 12. Comparison between the outputs of input MLPs and their best decoded counterparts (minimum-MSE selection among all decoders). HL refers to hidden layers.

TABLE I
HYPERPARAMETER SETTINGS FOR DIFFERENT LEVELS OF SPARSITY AND COMPACTNESS REGULARIZATION.

Penalty Level	λ_s	α	β
Small Penalty	1×10^{-5}	1×10^{-1}	1×10^{-4}
Medium Penalty	1×10^{-4}	4×10^{-1}	1×10^{-3}
Large Penalty	1×10^{-3}	4×10^{-1}	1×10^{-1}

Fig. 13 illustrates the effect of different regularization settings on the performance and sparsity of the resulting models. As expected, the curves align well with the penalty levels defined in Table I: stronger regularization (i.e., larger values of λ_s , α , and β) generally leads to lower non-zero weight counts but higher MSE. This confirms the trade-off between model compactness and predictive accuracy. In practice, medium penalty settings tend to offer a favorable balance, yielding compact architectures with minimal loss in performance.

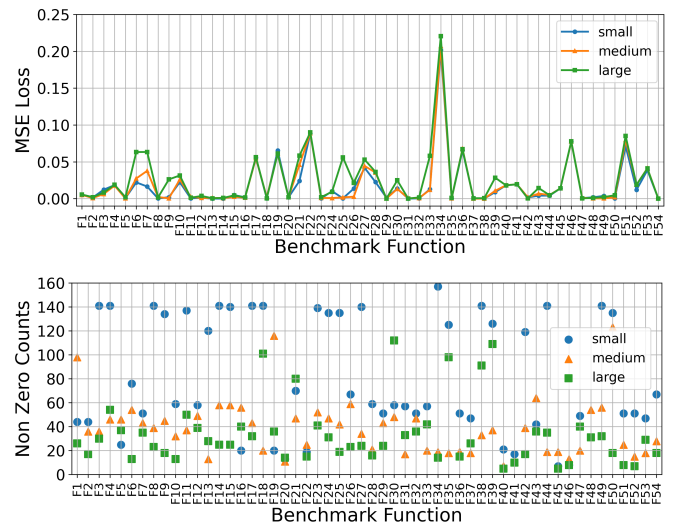


Fig. 13. Test MSE (top) and number of non-zero weights (bottom) for the best-performing networks under three different levels of sparsity and compactness regularization.

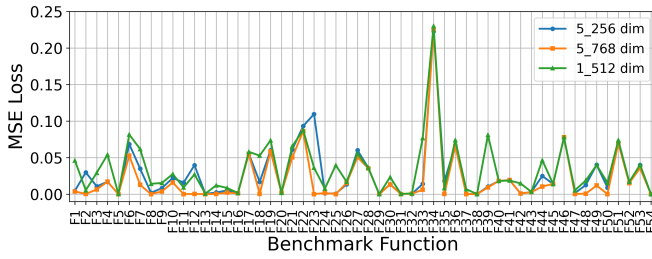


Fig. 14. Test MSE for the best MLPs found using embedding vectors of different dimensions on the CORNN dataset. Each curve corresponds to a specific embedding size: 5×768 , 5×256 , and 1×512 .

E. Change in size of the embedding space

To assess whether a large embedding dimensionality is necessary, we train autoencoders to embed 1–4 hidden layer MLPs with fixed structure: no bias terms, no activation functions, and exactly 5 neurons per layer. Each autoencoder is trained for 50 epochs, with 640,000 sampled MLPs per epoch. Fig. 14 compares performance on all regression tasks across different embedding sizes. In nearly all tasks, the 5×768 embedding yields lower or equal MSE loss compared to smaller alternatives (5×256 and 1×512). This suggests that a sufficiently large embedding space is beneficial for capturing functional variations in MLPs. Accordingly, we use a 7×768 embedding in our main experiments.

F. Compression of networks and variable input/output size

It is possible to compress large MLPs into smaller ones using the existing embedding space, without requiring deeper autoencoders. The key idea is that a deep network can be decomposed into smaller sub-networks connected in sequence, each of which can be individually compressed using the autoencoder. As a proof of concept, we compress a 9-hidden-layer MLP into a 5-hidden-layer MLP by splitting it into two sub-networks and compressing each with a lightweight 4-to-2 autoencoder. This autoencoder is trained on MLPs with leaky ReLU activations, 7 neurons per layer, and no biases.

Importantly, our matrix-based representation supports varying input and output sizes by updating the second-channel mask (see Fig. 3). This flexibility allows us to compress the first 4-layer MLP with input size 2 and output size 7, and the second with input size 7 and output size 1.

The compression is achieved by optimizing in the latent space of the 4-to-2 autoencoder for each sub-network. As shown in Fig. 15, the output of the compressed 5-layer MLP closely matches that of the original 9-layer MLP, demonstrating that large networks can be effectively approximated using SWAT-NN without needing to retrain a deeper autoencoder that matches the size of the original large network.

VI. CONCLUSION

We presented SWAT-NN, a novel framework that simultaneously optimizes both neural architectures and their weights within a universal and continuous embedding space. Through

extensive experiments on all 54 regression tasks in the CORNN dataset, we demonstrated that SWAT-NN consistently yields performant networks with desirable sparsity and compactness, achieving comparable or better accuracy while producing more compact and sparse neural networks than state-of-the-art methods.

While this work focuses on MLPs, the SWAT-NN framework opens up several future research directions. In particular, extending the approach to more complex neural network families such as Temporal Convolutional Networks (TCNs), Convolutional Neural Networks (CNNs), and Recurrent Neural Networks (RNNs) could enable broader applicability.

REFERENCES

- [1] P. Ren, Y. Xiao, X. Chang, P.-Y. Huang, Z. Li, X. Chen, and X. Wang, "A comprehensive survey of neural architecture search: Challenges and solutions," *ACM Computing Surveys (CSUR)*, vol. 54, no. 4, pp. 1–34, 2021.
- [2] T. Elsken, J. H. Metzen, and F. Hutter, "Neural architecture search: A survey," *Journal of Machine Learning Research*, vol. 20, no. 55, pp. 1–21, 2019.
- [3] B. Zoph and Q. V. Le, "Neural architecture search with reinforcement learning," *arXiv preprint arXiv:1611.01578*, 2016.
- [4] Y. Liu, Y. Sun, B. Xue, M. Zhang, G. G. Yen, and K. C. Tan, "A survey on evolutionary neural architecture search," *IEEE transactions on neural networks and learning systems*, vol. 34, no. 2, pp. 550–570, 2021.
- [5] K. O. Stanley and R. Miikkulainen, "Evolving neural networks through augmenting topologies," *Evolutionary computation*, vol. 10, no. 2, pp. 99–127, 2002.
- [6] B. Baker, O. Gupta, N. Naik, and R. Raskar, "Designing neural network architectures using reinforcement learning," *arXiv preprint arXiv:1611.02167*, 2016.
- [7] Z. Zhong, J. Yan, W. Wu, J. Shao, and C.-L. Liu, "Practical block-wise neural network architecture generation," in *Proceedings of the IEEE conference on computer vision and pattern recognition*, 2018, pp. 2423–2432.
- [8] K. O. Stanley, D. B. D'Ambrosio, and J. Gauci, "A hypercube-based encoding for evolving large-scale neural networks," *Artificial life*, vol. 15, no. 2, pp. 185–212, 2009.
- [9] X. Yao, "Evolving artificial neural networks," *Proceedings of the IEEE*, vol. 87, no. 9, pp. 1423–1447, 1999.
- [10] Y. Chen, G. Meng, Q. Zhang, S. Xiang, C. Huang, L. Mu, and X. Wang, "Renas: Reinforced evolutionary neural architecture search," in *Proceedings of the IEEE/CVF conference on computer vision and pattern recognition*, 2019, pp. 4787–4796.
- [11] H. Liu, K. Simonyan, and Y. Yang, "Darts: Differentiable architecture search," *arXiv preprint arXiv:1806.09055*, 2018.
- [12] S. Santra, J.-W. Hsieh, and C.-F. Lin, "Gradient descent effects on differential neural architecture search: A survey," *IEEE Access*, vol. 9, pp. 89 602–89 618, 2021.
- [13] S. Xie, H. Zheng, C. Liu, and L. Lin, "Snas: stochastic neural architecture search," *arXiv preprint arXiv:1812.09926*, 2018.
- [14] H. Cai, L. Zhu, and S. Han, "Proxylessnas: Direct neural architecture search on target task and hardware," *arXiv preprint arXiv:1812.00332*, 2018.
- [15] K. M. Malan and C. W. Cleghorn, "A continuous optimisation benchmark suite from neural network regression," in *International Conference on Parallel Problem Solving from Nature*. Springer, 2022, pp. 177–191.
- [16] J. Li, Y. Liu, J. Liu, and W. Wang, "Neural architecture optimization with graph vae," *arXiv preprint arXiv:2006.10310*, 2020.
- [17] Z. Huang, M. Montazerin, and A. Srivastava, "Simultaneous weight and architecture optimization for neural networks," *arXiv preprint arXiv:2410.08339*, 2024.
- [18] A. Radford, J. Wu, R. Child, D. Luan, D. Amodei, I. Sutskever *et al.*, "Language models are unsupervised multitask learners," *OpenAI blog*, vol. 1, no. 8, p. 9, 2019.
- [19] T. Zhang, S. Ye, K. Zhang, J. Tang, W. Wen, M. Fardad, and Y. Wang, "A systematic dnn weight pruning framework using alternating direction method of multipliers," in *Proceedings of the European conference on computer vision (ECCV)*, 2018, pp. 184–199.

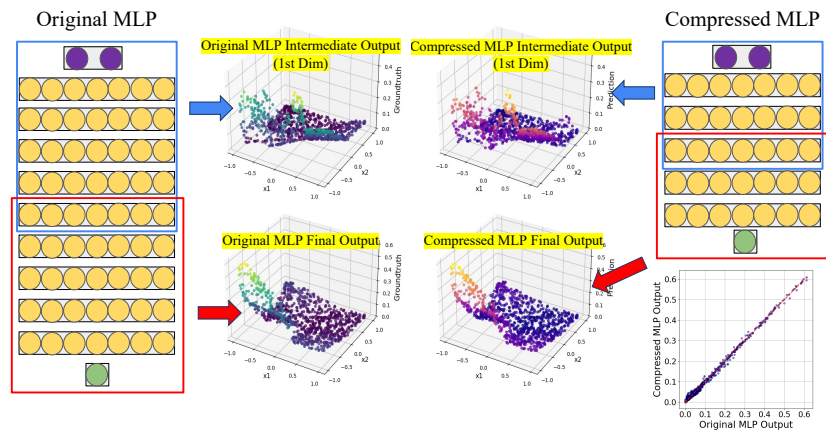


Fig. 15. Intermediate and final outputs of the original vs. compressed MLP. The compressed 9 hidden layer MLP closely replicates both internal representations and final predictions of the original 9 hidden layer MLP. This approach also demonstrates SWAT-NN's ability to train variable input/output MLPs.